Fuel 381 (2025) 133373

Contents lists available at ScienceDirect

Fuel

journal homepage: www.elsevier.com/locate/fuel

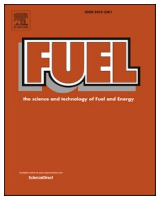

Full Length Article

Why does coal permeability time dependency matter?

Yaoyao Zhao [a], Yixin Zhao [b], Jishan Liu [c,*], Mingyao Wei [d], Zhihong Zhao [a], Derek Elsworth [e]

[a] Department of Civil Engineering, Tsinghua University, Beijing 100084, China
[b] School of Energy & Mining Engineering, China University of Mining and Technology, Beijing 100083, China
[c] School of Engineering, The University of Western Australia, 35 Stirling Highway, WA 6009, Australia
[d] National and Local Joint Engineering Laboratory of Internet Application Technology on Mine, IoT Perception Mine Research Center, China University of Mining and Technology, Xuzhou, Jiangsu 221116, China
[e] Department of Energy and Mineral Engineering, G3 Center and Energy Institute, The Pennsylvania State University, University Park, PA 16802, USA

ARTICLE INFO

Keywords:
Sorption-induced strain
Coal permeability
Gas injection
Multimodal evolution

ABSTRACT

Permeability is a key property of coal for both natural gas extraction from and/or carbon dioxide sequestration in coal seams. It is normally defined as a function of effective stress. A fundamental assumption is that both gas pressure and its associated strains are independent of time. In these efforts, the gas diffusion process and its associated volumetric transformation between fractures and matrices were rarely considered. In this study, a special apparatus was setup to continuously monitor/calculate all essential variables under controlled gas injection conditions, including (1) coal permeability, (2) overall strain, (3) fracture strain, and (4) matrix strain. Two tests were conducted: (1) CO_2 injection test and helium test for reference. Both were conducted under the condition of constant effective stresses. In the CO_2 test, permeability experienced four distinct stages: (1) increase due to fracture pressure, (2) decrease due to local matrix swelling, (3) recovery due to matrix swelling expansion, and (4) stability due to equilibration between fractures and matrices over a period of 90 days. Based on these observations and analysis, we conclude that coal permeability evolves even under constant injection conditions. This suggests that coal permeability is time-dependent even under constant gas extraction/injection conditions and this dependency must be considered during natural gas production or gas sequestration in coal seams.

1. Introduction

Natural gas can be extracted from and carbon dioxide can be sequestered in coal seams [1–3]. Due to the nature of dual porosity nature [4], coal has a significant sorption capacity for sorptive gases such as carbon dioxide and natural gas [5,6]. The fracture network is the main channel for flow while the pores in the matrices are the main space for gas storage [7]. Coal permeability is an important parameter for both natural gas extraction and gas storage [8–11]. It is controlled by effective stresses [12–14] which are affected by in-situ stress, pore pressure and by gas sorption [15–17]. The law of effective stress [14] indicates that the permeability does not change if the effective stress is constant [18]. However, many experimental results have shown that coal permeability changes with the increase of gas injection pressure under the condition of constant effective stress [2,19–21].

In the last decade, several models have been developed to address this contradiction between measurements and predictions [22–24]. Alternative tests have also been conducted to see how coal permeability responds to the constant confining pressure [25–32], constant pore pressure [33], uniaxial compression [34–37], constant effective stress [21,26,38–42], and constant volume. Theoretical models include the single-weight porous media models [8,43–45], double-porosity media models [46,47], permeability models under steady state conditions [43], permeability models under variable stress conditions [8], and the permeability models considering the interaction between matrix and fracture [47,48]. These models were applied to explain the above contradiction by linking the contradiction to anisotropy and heterogeneity [49–51] of coal and the variations in the Biot coefficient [52,53], elastic modulus [54–56], and gas sorption [57–59] at different gas pressures. In recent studies, this contradiction has been linked to the non-uniform deformation of coal [18,21,26,45,48,60–63]. However, all of the above theoretical models are based on the same assumption that coal permeability is controlled by the overall strain other than the fracture strain [19,64,65]. The permeability of coal matrices is several orders of magnitude lower than that of fractures. This is why previous studies focus on the fractures network, but neglect the dynamic changes

* Corresponding author.
E-mail address: jishan.liu@uwa.edu.au (J. Liu).

https://doi.org/10.1016/j.fuel.2024.133373
Received 28 May 2024; Received in revised form 2 October 2024; Accepted 3 October 2024
Available online 7 October 2024

in the gas pressure and sorption in matrices [48,58,66]. When the role of matrices is ignored, the time dependency of coal permeability cannot be captured.

In addition, the transient step method [35,67], steady state method [34,68,69], and periodic oscillation method [70,71] have also been used to measure the permeability of coal samples. These methods measure the permeability of coal samples under varied injection conditions. Wei et al. [72] conducted a long-term test under the same injection conditions. However, essential variables such as the radial strain, overall strain, and fracture strain were not measured. Based on the observed evolution of the permeability, a conceptual permeability model was developed to divide the permeability into four stages: a rapid increase, decline, slow rebound and steady state during the process of gas injection [72]. This work is a logical extension of our previous work. The objectives are to further understand (1) how does the competitive relationship between the gas pressure changes and sorption controls the permeability evolution in the process of long-term gas injection? (2) how do the matrix and fracture deformation interact dynamically? (3) what is the relationship between the permeability evolution and the differential deformation between the fractures and coal bulk? To achieve these goals, a long-term test under the same gas injection conditions was completed over a period of 90 days. All of the observations were analyzed.

2. Experimental methods

This experiment was divided into two parts: helium injection for 40 days (He-group) and carbon dioxide injection for 90 days (CO_2-group). The coal sample was continuously injected with helium or carbon dioxide at a fixed gas pressure under a constant confining pressure of 6 MPa. The coal sample was injected with helium at a pressure of 3 MPa for 40 days. After vacuuming the sample for10 days, the confining pressure remained unchanged, and the coal sample was subjected to continuous injection of carbon dioxide for a duration of 90 days at the gas injection pressure of 3 MPa. The permeability, overall strain and fracture strain of the sample were continuously measured over the course of the experiment. In addition, the experimental system was used to measure the elastic modulus and Poisson's ratio of the coal sample to provide a more comprehensive set of experimental data.

2.1. Experimental system and coal core

The equipment used in this experiment is thermal-hydro-mechanical-chemical (THMC) test system (Fig. 1), which was improved based on the experimental system described in our previous studies [21,73].

In this experiment, the sample was low permeability anthracite coal ($d \times l$: 50 mm × 35 mm) from the Licun coal mine in China (Fig. 2). The mass and density of the sample were 281.18 g and 1.413 g•cm^{-3}, respectively. Compositions of the coal sample were shown in Table 1.

2.2. Permeability and strain measurement experiment

As mentioned above, the experiment was divided into two parts: a helium injection experiment (for 40 days) and a carbon dioxide injection experiment (for 90 days). The evolution curves of the upstream and downstream pressures are shown in Fig. 3. It is unfortunate that we were unable to measure the sorption curve of the carbon dioxide on the coal sample under the isothermal condition in this experiment due to the absence of a flowmeter at the upstream pipeline of the test system.

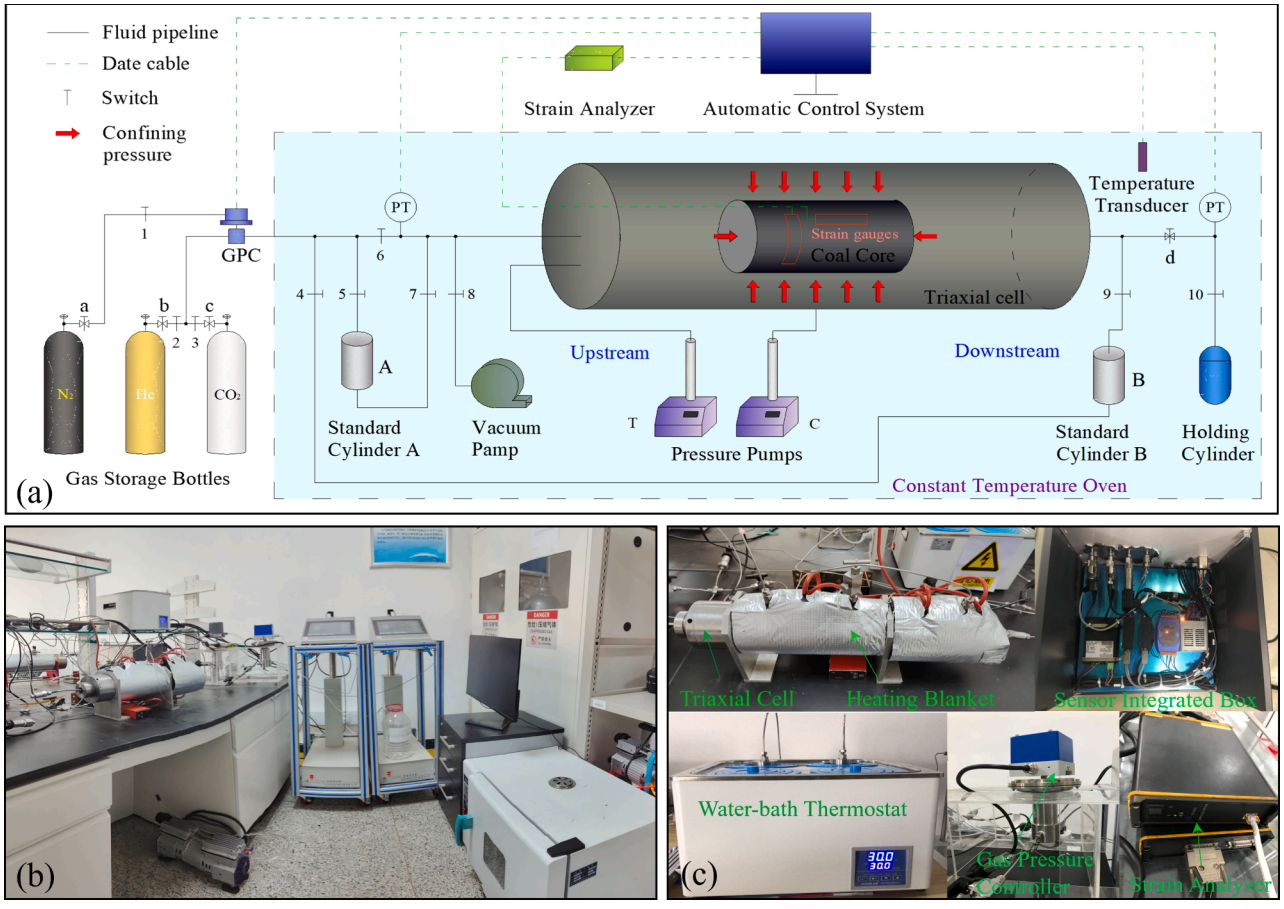

Fig. 1. THMC test system [73]. (a) Schematic diagram; (b) physical photograph; (c) partial equipment photographs.

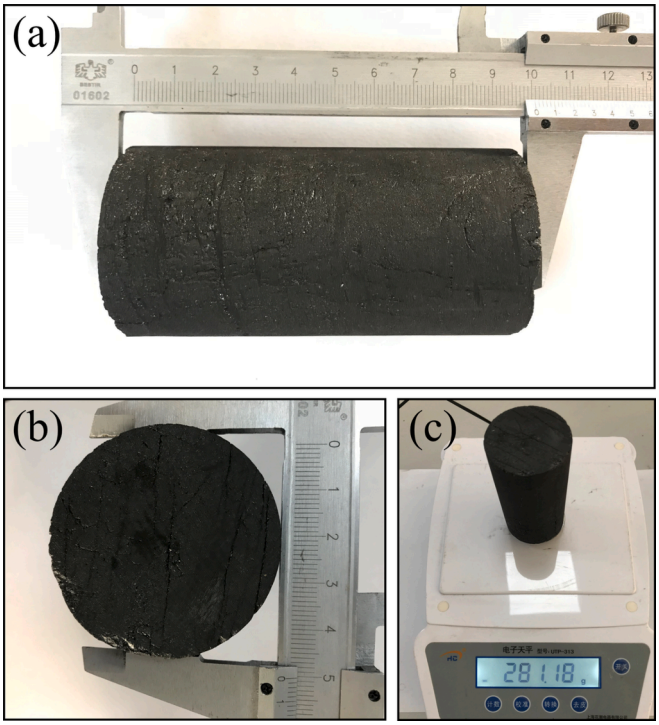

Fig. 2. Photographs of the sample.

Nevertheless, since this study mainly focused on the evolution of the coal permeability and strains, we believe that the absence of the isothermal sorption curve will not impede our research. The specific experimental methods are described below.

In this experiment, the sample was continuously injected helium and carbon dioxide for 40 days and 90 days under the condition of constant confining pressure of 6 MPa. The test temperature was a constant of 30 ℃ controlled by the temperature control system. The necessary preparations were completed prior to commencing the test, including measure gas tightness, dry sample, affix strain gauges (Fig. 4**a**), cover with heat shrinkable tube (Fig. 4**b**) and tinfoil paper (Fig. 4**c-d**), load the sample into the triaxial holder and adjust the confining pressure loading on the sample to 6 MPa, vacuum test system for 24 h, adjust and maintain the system temperature to 30 ℃. After that, we completed two experiments of the He-group and the CO_2-group. The experimental procedures are outlined as follows.

(1) Inject helium into the coal sample for 40 days (He-group). First, the switches 4–6 and 10 were turned off and the switches 7–9 were turned on. The vacuum pump was used to extract the gas in the system for 24 h. After that, the switch 3, 4, 8 and 10 were turned off and the switches 1, 2, 5–7 and 9 were turned on. The gas pressure controller was used to inject helium gas with a pressure of 3 MPa into the experiment system. When the downstream pressure was equal to the upstream pressure, the switches 3, 4, 6–8 and 10 were turned off, and the time was recorded as t_0. The gas pressure controller was used to inject helium with a pressure of 3.2 MPa into the upstream standard cylinder A. The switches 3–6, 8 and 10 were turned off and the switches 7, 9 were turned on. When the downstream pressure was equal to the upstream pressure, the time was recorded as t_1. And then, the changes of upstream and downstream gas pressures were continuously observed for 2 h, and the time was recorded as t_2. After that, the switches 3, 4, 6–8 and 10 were turned off and the switches 1, 2, 5 and 9 were turned on, and the gas pressure was used to adjust the gas pressure of the upstream standard cylinder A to 2.8 MPa. The switches 3–6, 8 and 10 were turned off and the switches 7 and 9 were turned on. When the downstream pressure was equal to the upstream pressure, the time was recorded as t_3. And then, the changes of upstream and downstream gas pressures were continuously observed for 2 h, and the time was recorded as t_4. The operation during the time period t_0-t_5 is a measurement cycle. And we repeated the measurement cycle for the 40 days.

(2) Inject carbon dioxide into the sample for 90 days (CO_2-group). First, the switches 4–6 and 10 were turned off and the switches 7–9 were turned on. The vacuum pump was used to extract the gas in the system for 240 h. After that, we repeated the measurement cycle of the step of He-group above for 90 days, except that the helium was replaced by carbon dioxide.

The experiment was conducted for a total duration of 140 days, including 40 days of He-group test, 10 days of vacuum and 90 days of CO_2-group test. They are not planned before the experiment, but depend on the time required for the evolution of coal permeability and deformation to reach the final stability during the test process.

The method for assessing the balance of gas pressure between the upstream and downstream is as follows: the upstream gas pressure is P^I_{up0} after obtaining a positive pulsating pressure (about 0.2 MPa), while the downstream gas pressure is P^I_{dn0}. Driven by the pressure gradient ($P^I_{up0} - P^I_{dn0}$), the gas in the standard cylinder A of upstream flow to the standard cylinder B of downstream, until the upstream and downstream pressures are equal to the equilibrium pressure P^I_e. We judge that the gas pressure in the upstream and downstream reaches the balance at this time. The above stage is the positive pulse stage ($P^I_{up0} > P^I_{dn0}$). After that, the upstream obtaining a negative pulsating pressure (about −0.2 MPa), and the upstream gas pressure is P^E_{up0}, while the downstream gas pressure is P^E_{dn0}. Driven by the pressure gradient ($P^E_{dn0} - P^E_{up0}$), the gas in the standard cylinder B of downstream flow to the standard cylinder A of upstream, until the upstream and downstream pressures are equal to the equilibrium pressure P^E_e. The above stage is the negative pulse stage. In

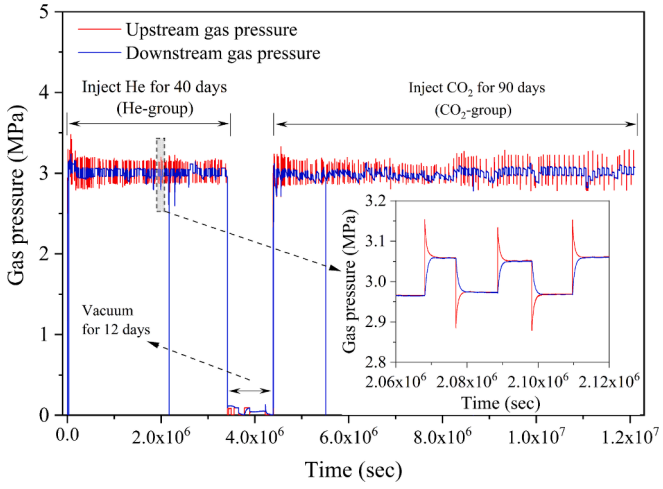

Fig. 3. Evolution curves of the upstream and downstream pressures.

Table 1
Compositions of the coal sample [26].

Type	Size (cm)		Proximate analysis (mass %)		Ultimate analysis (mass %)							
	Diameter	Length	Volatile content	Ash content	C	O	Al	Si	S	N	Fe	P
Bituminous coal	5.02	10.06	34.87	19.10	80.4	12.9	1.7	1.7	1.17	1.3	0.7	0.039

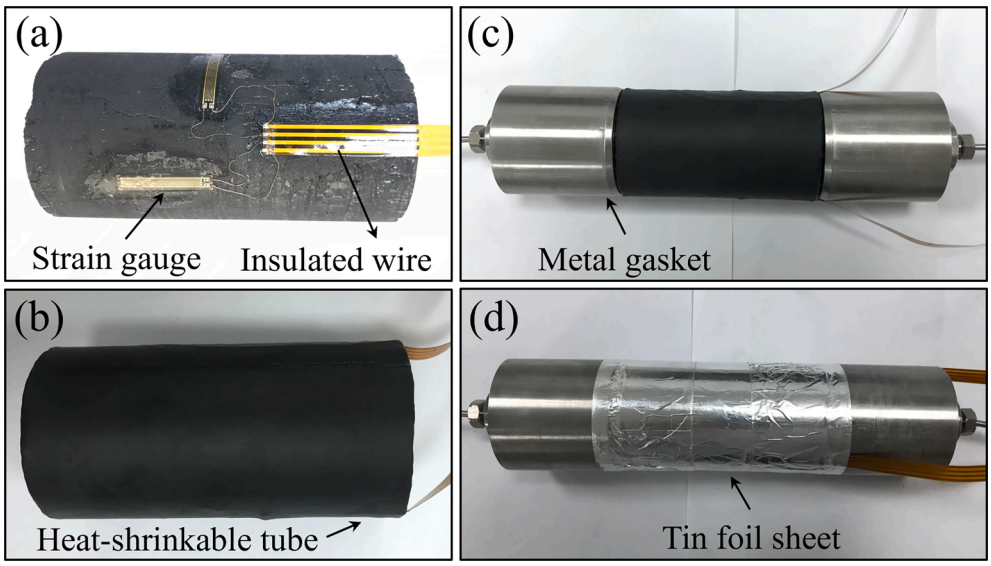

Fig. 4. Preparations of coal sample before measurement. (a) Sticked four strain gauges; (b) wrapped in a heat shrink tube; (b) sandwiched between two metal gaskets; (d) attached a tinfoil paper.

this experiment, a test cycle consists of a positive pulse stage and a negative pulse stage ($P^E_{dn0} > P^E_{up0}$). The values of coal permeability and fracture volume measured in this test cycle are the average values measured from the two stages.

In this experiment, the coal permeability, overall strain and fracture strain were measured by the transient method, 1/4 bridge strain gauges and gas expansion method respectively. Please refer to our previously published researches [21,73] for specific measurement principle. It is worth noting that the the measured fracture volume is the aggregate of the pore and fracture volumes that contribute to the gas fluid in the experiment.

2.3. Mechanical parameters measurement experiment

The mechanical parameters in the measurement experiments on the sample were determined using the coal gas multi-process coupling test system. The experiment measured the elastic modulus and Poisson's ratio of the coal sample under the uniaxial condition. The elasticity modulus and Poisson's ratio of coal are the basic mechanical parameters of coal that play crucial roles in the modelling of both uniaxial and triaxial boundary conditions [8,60,74]. Therefore, it is imperative to consider these parameters in subsequent investigations that aim to simulate this experiment. The elastic modulus and Poisson's ratio of the sample were calculated by observing the change using the strain gauge on the side of the sample under the condition of a continuous increase in the axial pressure. The experimental steps were as follows: (1) the experimental system was checked to ensure that the experimental equipment was under normal conditions. (2) The surface of the coal sample was ground flat using fine sandpaper, and two strain gauges were closely attached to the side of the coal sample. The two strain gauges were oriented vertical and parallel to the axial direction of the coal sample. Then, the coal sample was encased in a rubber jacket and loaded into the triaxial cell. (3) The flow of the injected pressure fluid was controlled by the pressure pumps, so the coal sample was gradually compressed in the axial direction. During this process, the axial pressures on the coal sample were recorded by the pressure pump, and the axial and circumferential displacements of the coal sample were recorded by the strain analyser. When the axial pressure reached 15 MPa, the axial pressure pump was closed, and the measurement experiment of mechanical parameters was complete.

The elastic modulus of the sample was obtained by the relationship between the measured axial strain and axial loading pressure:

$$E = \frac{\Delta\sigma_a}{\Delta\varepsilon_a} \tag{1}$$

where, E is the elastic modulus of the sample. $\Delta\sigma_a$ is change of axial pressure. $\Delta\varepsilon_a$ is the change of axial strain. The Poisson's ratio was obtained by the ratio of radial strain and axial strain:

$$\nu = \frac{\Delta\varepsilon_r}{\Delta\varepsilon_a} \tag{2}$$

where, ν is the Poisson's ratio of the sample. $\Delta\varepsilon_r$ is the change of radial strain.

3. Experimental results

In this study, the permeability, overall strain and fracture strain of the sample were continuously measured and we defined the swelling strain as positive and the compressive strain as negative. The experimental results are presented in the following sub-sections.

3.1. Changes in permeability with gas injection time

Using the above permeability measurement method, we observed the permeability values of the coal sample during helium injection for 40 days and carbon dioxide injection for 90 days. It should be noted that the permeability values during 0–2 h were fitted by the relationship between the gas pressure and time, and we assumed that the permeability value fitted during 0–400s was the initial permeability. In this experiment, the initial permeability values of the He group and CO_2 group were 72.472 μD and 67.248 μD, respectively. The permeability ratios are shown in Fig. 5.

The results of the permeability ratio measurements clearly demonstrate an initial rapid increase in the sample permeability (from 1 to 2.46), followed by stabilization at a certain value (2.36) as the helium injection time increased. However, with increasing carbon dioxide injection time, the permeability experienced four stages: a rapid increase, decline, slow rebound, and steady state. The maximum permeability ratio was 2.48, and the final stable permeability ratio was 1.18. The maximum permeability ratios of the sample were similar under the helium and carbon dioxide injection conditions, but the final stable permeability ratios were significantly different. In addition, the permeability gradually decreased during the period of 40–90 days for

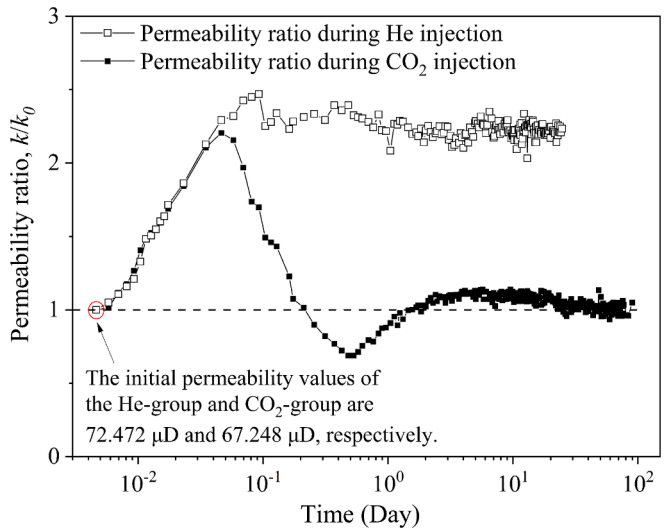

Fig. 5. Measured results of permeability during gas injection.

the CO_2 injection, which was likely due to the pore and fracture shrinkage induced by the creep effect under the triaxial loading condition. By comparing the initial permeability values of the He-group and CO_2-group, it was found that the initial permeability value of the CO_2-group was 67.248 μD, which was slightly lower than that of the He-group (72.472 μD). However, considering that the difference ratio ([72.472–67.248]/72.472 = 7.2 %) was less than 10 %, we believe that despite not completely eliminating the creep effect from affecting results in this study, its impact on the experimental outcomes for the CO2-group are acceptable.

3.2. Overall changes in strain with gas injection time

The overall strain values of the sample were continuously measured by the strain analyser and four strain gages (Fig. 6). In both the helium and carbon dioxide injection experiments, the overall strains changed in three stages: a rapid increase, slow increase, and steady state. In the rapid increase stage, the main factor causing the coal bulk swelling was that the gas pressure of the fracture increased from 0 MPa to 3 MPa, resulting in a similar overall strains of the sample in the two groups of experiments. In the slow increase stage, the overall strain in the He-group was contributed by the change in the matrix pore pressure, while the overall strain in the CO_2-group was contributed by the changes in the matrix pore pressure and sorption. Therefore, the overall strain in the He-group was lower than that in the CO_2-group in the steady state stage. The overall strain values were less than 3 ‰, indicating that the overall volume expansion was weak in both the helium and carbon dioxide groups. We believe that there are two reasons for this result. (1) Different from the conventional sorption strain measurements under free expansion conditions (i.e., the confining pressure and gas pressure are equal), the coal sample used in this experiment was loaded in a triaxial loading environment with a confining pressure of 6 MPa, which significantly restricted the expansion of the bulk coal induced by the sorption and pore pressure. (2) The anthracite sample used in the experiments had a significant degree of fracture development. The deformation of the coal sample may have mostly been contributed by means of compression of the fractures, resulting in weak expansion of the coal sample. This finding is intriguing and diverges from previously reported experimental outcomes, and it indicates that the transition from local equilibrium to global equilibrium may be more complex and significance than expected, potentially providing an avenue for explaining the cause of the unsuccessful CO_2-enhanced coal bed methane (CO_2-ECBM) recovery in pilot field tests. The results of our study imply that not all of the CO_2-induced swelling strain contributes to the bulk strain. The contribution ratio is dependent on a set of factors, such as the fractures, matrix properties, and boundary conditions. Additionally, numerous reported experimental studies [75–78] have recorded strain values of coal samples significantly below the conventional strain of 3–5 % induced by sorption, and some even reported lower strains than the overall strain of 3 ‰ measured in our test. Therefore, current practices may overestimate the role of swelling strain in the bulk strain and may underestimate the role of matrixes in permeability evolution.

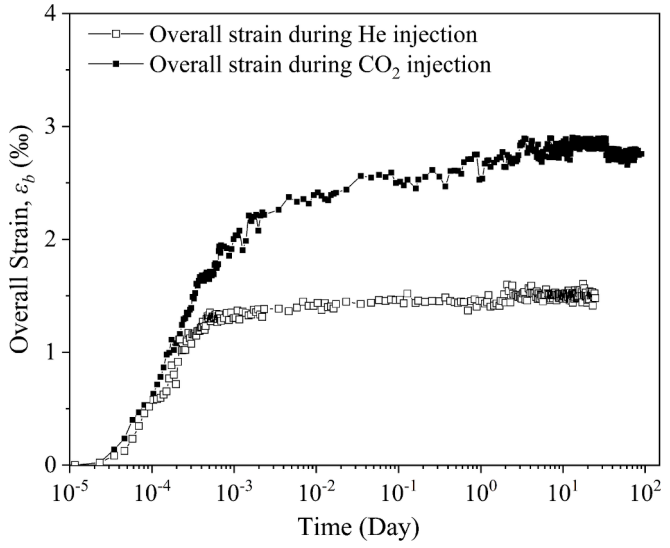

Fig. 6. Measured results of the overall strain during gas injection (the swelling strain is positive).

3.3. Changes in fracture volume and strain with gas injection time

In this experiment, we roughly measured the fracture volume of the sample and calculated the fracture strain using the change in fracture volume. Since the measurement of each fracture volume was conducted within 2–4 h, we obtained the first fracture volume when the gas injection time was 2 h. We assumed that the first fracture volume was the initial fracture volume. In this experiment, the initial porosity values of the He-group and CO_2-group were 4.45 % and 4.33 %, respectively. The measurement results of the fracture strain are shown in Fig. 7.

With increasing helium injection time, the fracture strain initially decreased and then stabilized. Different from the He-group, with increasing carbon dioxide injection time, the fracture strain initially decreased rapidly, rebounded after half a day, and finally stabilized within the range of −8.3 % to −10.6 %. Compared with the results of the He-group, i.e., that the fracture opening decreased gradually, the fracture strain result of the CO_2-group was contributed by the combined effects of the gas sorption and changes in gas pressure, leading to an initial decrease and then rebound. During the gas injection, the CO_2 diffused from the fractures into the pores of the surrounding matrix. In the earlier stage, the contributions of sorption to the changes in these parameters were much greater than those of the gas pressure. The matrix around the fracture expanded rapidly due to the increases in the sorption and pore pressure. Most of the expanded volume of the matrix was consumed by compressing the fracture volume, and a small part contributed to the overall volume expansion. In the swelling transition stage, the contributions of the sorption to the variations in the deformation and permeability were greater than those of the gas pressure. The migration of the edge of the gas-invaded area from the fracture to the sample boundary and the expansion of the matrix bridge were the main reasons for the variations.

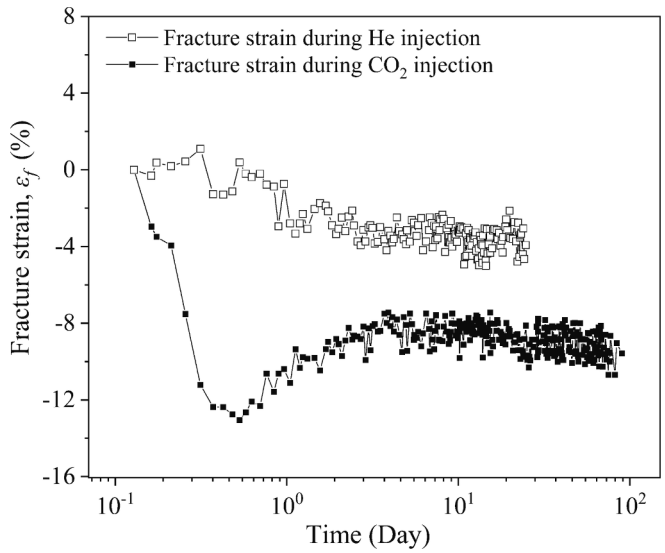

Fig. 7. Measured results of the fracture strain during gas injection (the compressive strain is negative).

3.4. Measurements of mechanical parameters

To obtain a comprehensive set of experimental data, the experimental system was used to measure the elastic modulus and Poisson's ratio of the sample. The stress–strain curves generated using the measurements are shown in Fig. 8, and the measurement results and geometric parameters of the sample are shown in Table 2. The elasticity modulus of the coal sample was 2433 MPa, and the Poisson's ratio was 0.2184 .

4. Analysis and discussion

Coal is a typical heterogeneous porous medium, and its internal structure and components are obviously heterogeneous, resulting in significant differences in the mechanical and seepage properties of different coal samples. Therefore, the results of the coal deformation and permeability evolution measured in experiments on different coal samples may have great differences or even be opposite. Regrettably, we have not completed more experiments on three or more coal samples to verify that the experimental results obtained apply to most coal samples. However, we believe that the significant value of this work exhibits the complete evolution of the permeability and overall strain of a coal sample during He and CO_2 injection. The experimental results indicate that it is difficult to achieve global equilibrium of coal samples in a short time, which is inconsistent with the majority of reported air permeability tests, that is, it takes 2–72 h for the coal sample to reach global equilibrium. The new findings of this study serve as a reminder for researchers to pay attention to the time dependency of permeability for gas flow in coal reservoirs.

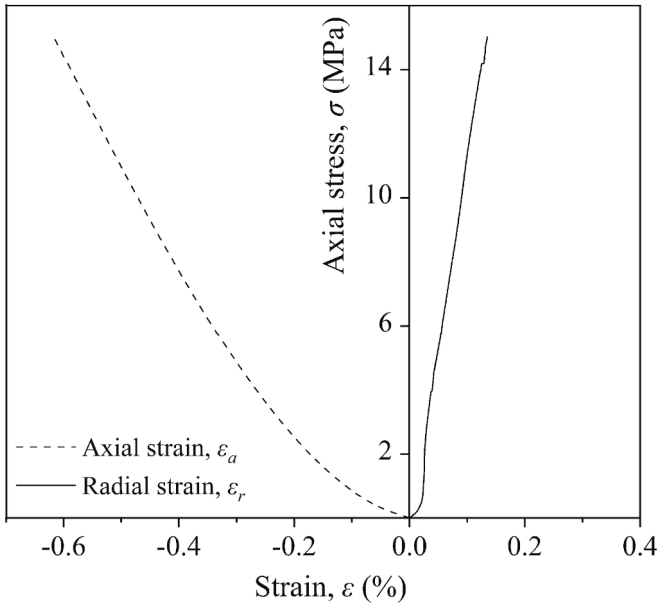

Fig. 8. The stress–strain curves of the sample (the swelling strain is positive).

Table 2
The parameters of the coal sample.

Parameter	Value
Length (mm)	99.1
Diameter (mm)	49.8
Weight (g)	263.0
Elasticity modulus (MPa)	2433
Poisson's ratio	0.2184

4.1. Competition between sorption and pore pressure

The deformation of the coal bulk, fractures, and matrix of the sample were controlled by the sorption and gas pressure changes during the gas flow in the fractures and matrix. Since helium is a non-adsorbent gas, there was no sorption to control the deformation during helium injection [79]. The pore pressure change in the fractures and matrix was the main factor controlling the deformation. In contrast, carbon dioxide is an adsorbent gas [80] and the changes in the pore pressure and sorption controlled the deformation and permeability during carbon dioxide injection [81]. In order to facilitate the study of the competition between the effects of the sorption and pore pressure changes on the permeability, we ignored the effect of the diffusion coefficient of the matrix caused by the changes in the internal structure during gas injection. The mechanical conditions for both groups were identical, and the same coal sample was used. We assumed that the creep effect exerted a similar influence on the experimental results of both groups and that the equal gas injection time and the pore pressure distribution in the sample in the two experiment groups were identical during the same gas injection time of 0–40 days. Based on the difference between the measured results of the CO_2-group and the He-group, the relationships between the measured values contributed by the sorption and pore pressure changes with gas injection time were obtained (Fig. 9**)**.

During the continuous injection of carbon dioxide into the sample, the changes in the permeability and strain occurred in four stages: the fracture expansion stage (0–0.06 days), local swelling stage (0.06–0.5 days), swelling transition stage (0.5–10 days), and global swelling stage (more than 10 days). These stages are based on the results of the evolution of the coal permeability during the CO_2 injection (black line in Fig. 9**a**) and were divided according to the peaks of the coal permeability changes and the corresponding time at which the coal permeability reached relative stability. There was competition between sorption and pore pressure in controlling the deformation and permeability in each stage, and we analysed this competition.

In the fracture expansion stage, the permeability and overall strain of the sample increased rapidly, and the changes contributed by the change in pore pressure were basically consistent with the changes in the sample, while there were no changes contributed by the sorption. The permeability and overall strain of the sample were almost completely contributed by the change in the pore pressure. The reason for this is that the permeability of the fractures was much greater than that of the matrix, and the gas pressure of the fractures increased rapidly and reached equilibrium first. The increase in the gas pressure of the fracture resulted in increases in the fracture volume, permeability (Fig. 9**a**), and

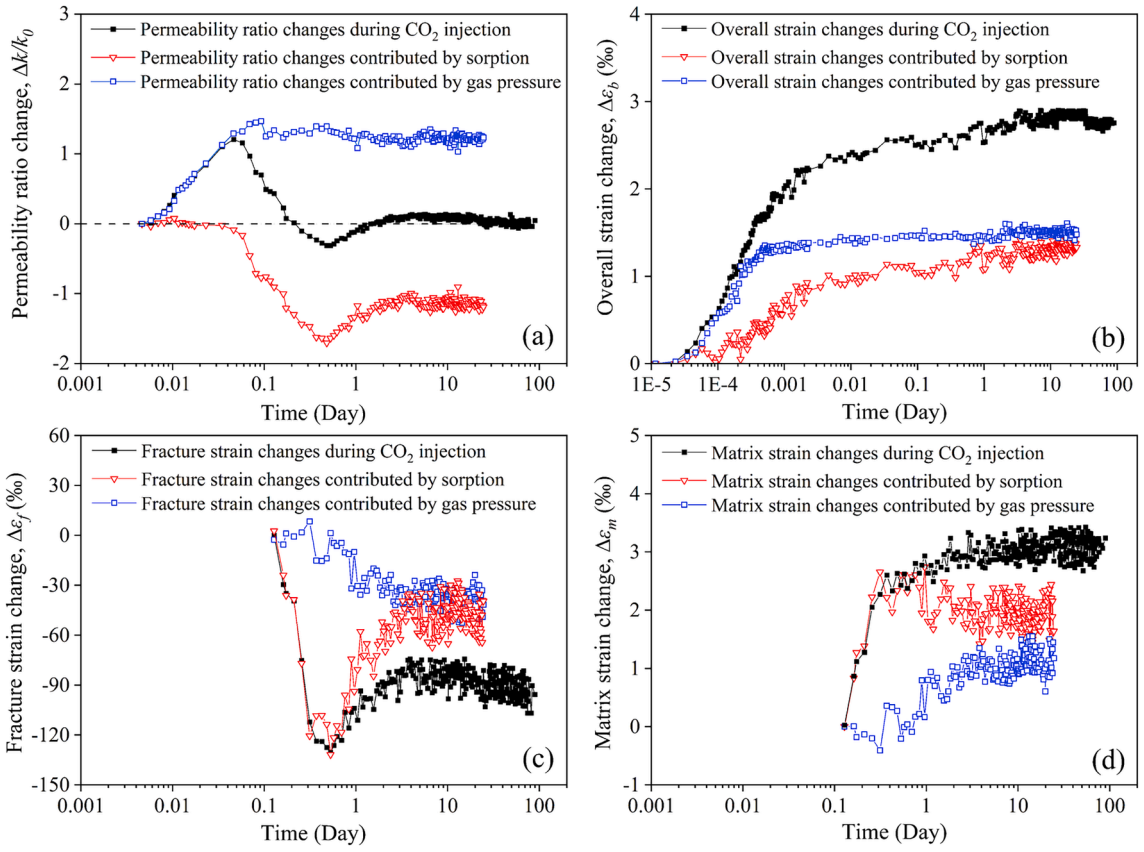

Fig. 9. Competition between the gas pressure and sorption during CO_2 injection. (a) Changes in the permeability ratio contributed by the gas pressure and sorption; (b) Changes in the overall strain contributed by the gas pressure and sorption; (c) Changes in the fracture strain contributed by the gas pressure and sorption; (d) Changes in the matrix strain contributed by the gas pressure and sorption.

overall volume (Fig. 9**b**). In the local swelling stage, the contributions of sorption to the changes in these parameters were much greater than those of the gas pressure. The matrix around the fractures expanded rapidly due to the increases in the sorption and pore pressure. Most of the expanded volume of the matrix was consumed by compressing the fracture volume (Fig. 9**c**), and a small part contributed to the overall volume expansion (Fig. 9**b**). In the swelling transition stage, the contributions of the sorption to the variations in the deformations and permeability were greater than those of the gas pressure. The migration of the edge of the gas-invaded area from the fractures to the sample boundary and the expansion of the matrix bridge were the main reasons for the variations. In the global swelling stage, there were no contributions of the pore pressure and sorption to the deformation and permeability. The pore pressure in the sample was uniform, and both the deformation and permeability were stable.

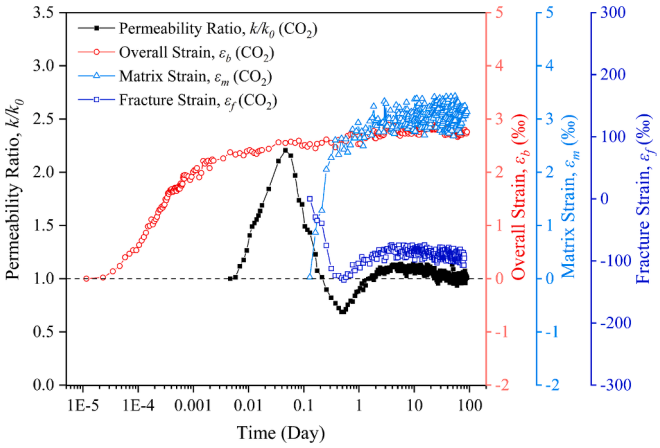

Fig. 10. The volume changes of the matrix and fractures during gas injection.

4.2. *Interaction between matrix and fractures during gas injection*

The evolution of the permeability is influenced by the interaction between the matrix and fractures [60]. The changes in the permeability ratio, overall strain, fracture strain, and matrix strain during carbon dioxide injection are shown in Fig. 10.

The expansion volume of the matrix contributed to the contraction of the fracture volume and the expansion of the overall volume. In the fracture expansion stage, the expansion of the fracture volume was almost entirely caused by the increase in the pore pressure. However, after the fractures reached equilibrium, the change in the fracture volume was caused by the interaction between the matrix and the fractures. In the local expansion stage, the volume of the matrix increased rapidly and the fracture volume decreased rapidly, demonstrating that the volume expansion of the matrix contributed to the contraction of the fracture volume. In the swelling transition stage, the contribution of the expansion of the matrix volume to the compression of the fracture volume decreased gradually, and the contribution to the expansion of the overall volume increased gradually. In contrast, the expansion of the matrix bridge between adjacent fractures led to the opening of the fractures. The above two reasons led to rebound of the fracture volume. In the global expansion stage, the matrix volume and fracture volume reached stability. It is noteworthy that the matrix volume increased rapidly in the local expansion stage, while the rate of the matrix volume increase decreased in the swelling transition stage. The reasons for this

were twofold. There were many secondary fractures around the fracture, which resulted in increased permeability of the matrix around the fractures. Moreover, the shape of the fractures was irregular, which facilitated the higher gas contact of the matrix around the fractures.

4.3. Control of coal heterogeneity on permeability

For the homogeneous hypothesis, the fracture network of the coal is uniformly distributed, and the matrix block is also homogeneous. Under this assumption, when the gas pressure reaches equilibrium in the coal sample, the bulk coal, fractures, and matrix expand synchronously. The overall strains, fracture strain, and matrix strain are always equal, and the porosity of the coal sample (the ratio of the fracture volume to the bulk volume) remains constant. Based on the cubic law, the coal permeability is also constant. However, the coal sample is a double porosity medium with obvious heterogeneity. The differences between the fracture and matrix are mainly reflected in the mechanical properties and sorption characteristics. Furthermore, the permeability of the matrix is several orders of magnitude lower than the permeability of the fractures. There is an obvious time-lag between the gas migration in the fractures and matrix during the process of gas injection. Under the combined action of these phenomena and the differences in the mechanical properties and sorption, there are discernible disparities among the fracture strain, matrix strain, and overall strain. In this paper, three types of differential deformation indexes are defined as the ratio of the fracture strain to the overall strain, including the global differential deformation index, sorption differential deformation index, and gas pressure differential deformation index.

$$f_{het} = \frac{\varepsilon_f}{\varepsilon_b} \tag{3}$$

$$f^s_{het} = \frac{\varepsilon^s_f}{\varepsilon^s_b} \tag{4}$$

$$f^g_{het} = \frac{\varepsilon^g_f}{\varepsilon^g_b} \tag{5}$$

where f_{het} is the global differential deformation index. f^s_{het} is the sorption differential deformation index. f^g_{het} is the gas pressure differential deformation index. ε^s_f is the fracture strain contributed by the sorption. ε^g_f is the fracture strain contributed by the changes in the gas pressure. ε^s_b is the overall strain contributed by the sorption. ε^g_b is the overall strain contributed by the changes in the gas pressure. These differential deformation indexes reflect the differential deformation degree of the coal. The absolute values of the difference between the differential deformation indexes and one are positively correlated with the degree of heterogeneity and the disequilibrium of the internal pore pressure. If the coal sample is homogeneous and the internal pore pressure is balanced, the values of the differential deformation indexes are one.

In this study, we substituted the overall strain and fracture strain into **Eqs. (3)–(5)** to obtain the global differential deformation index, sorption differential deformation index, and gas pressure differential deformation index (Fig. 11). There were obvious differences between the global, sorption, and gas pressure differential deformation indexes during the carbon dioxide injection. In the local expansion stage, the differential deformation between the bulk coal and fractures decreased gradually due to the changes in the gas pressure. The differential deformation increased rapidly due to the sorption. The influence of sorption on the differential deformation was much greater than that of the gas pressure, so the differential deformation between the bulk coal and fractures increased. In the swelling transition stage, the differential deformation between the bulk coal and the fractures occurred because the changes in the gas pressure still decreased gradually. However, the differential deformation caused by the sorption rebounded and decreased. The global differential deformation index decreased under the combined action of the sorption and gas pressure. In the stage of global expansion, the three differential deformation indexes were stable. The pore pressure of the sample reached a uniform state. Fig. 11 clearly illustrates that the trend of the changes in the permeability was basically the same as that of the changes in the global differential deformation index, which confirms that the differential deformation indexes reflected the variations in the permeability during the gas injection.

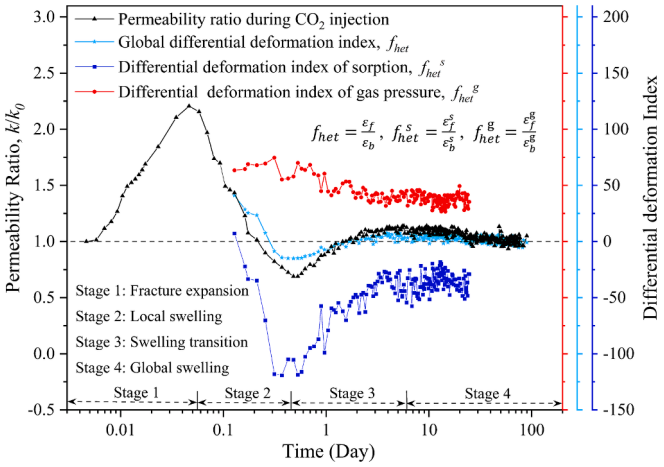

Fig. 11. The relationship between the differential deformation indexes and permeability. f_{het} is the global differential deformation index. f^s_{het} is the sorption differential deformation index. f^g_{het} is the gas pressure differential deformation index. ε^s_f is the fracture strain contributed by sorption. ε^g_f is the fracture strain contributed by changes in the gas pressure. ε^s_b is the overall strain contributed by sorption. ε^g_b is the overall strain contributed by the changes in the gas pressure.

5. Conclusions

In this study, we demonstrated that the equilibration process between the coal matrices and fractures is the reason why the coal permeability changes as a function of time even under the constant effective stress condition. This conclusion is supported by a complete set of long-term experimental data, including data on the permeability, overall strain, and fracture strain. Based on our experimental results, the following specific conclusions were drawn.

(1) Coal permeability was a function of the fracture local strain. Although the fracture effective stress was constant during gas injection, the strain changed due to the diffusion of gas from the fractures into the matrices. The diffusion process was time dependent and lasted longer than 90 days. Therefore, the equilibration process between the matrices and fractures must be considered.

(2) The coal permeability during CO_2 injection under constant effective stress exhibited multimodal characteristic, and it occurred in four distinct stages: an increase due to the fracture pressure, a decrease due to local matrix swelling, recovery due to matrix swelling expansion, and stability due to equilibration of the fractures and matrixes. During the permeability increase stage, all of the changes were confined within the fracture system. The fracture system was in equilibrium. During the permeability decline stage, dynamic changes took place in the matrix system, but these changes were confined within the near fracture field. During the permeability recovery stage, the dynamic changes in the matrix system propagated from the near to far fracture field. During the stable permeability stage, equilibrium was reached between the coal matrices and fractures.

(3) In the stable permeability stage, the measured permeability remained unchanged under a constant effective stress. This is consistent with the effective stress principle. The principle is valid only when equilibrium is reached between the coal matrices and fractures. Under this condition, the coal swells uniformly. Therefore, uniform swelling has no impact on the coal permeability. This conclusion implies that the discrepancy between the assumption of uniform swelling and the non-uniform reality is responsible for the contradiction between experimental measurements and theoretical predictions.

These findings demonstrate that the interaction between coal and gas undergoes a prolonged and dynamic evolution process. This process may be amplified to several years or decades for both natural gas extraction from and gas storage in coal seams. Therefore, the time dependency of coal permeability is significant.

CRediT authorship contribution statement

Yaoyao Zhao: Writing – original draft, Methodology, Investigation, Formal analysis, Data curation, Conceptualization. **Yixin Zhao:** Supervision, Resources, Conceptualization. **Jishan Liu:** Writing – review & editing, Supervision, Funding acquisition, Conceptualization. **Mingyao Wei:** Methodology, Data curation. **Zhihong Zhao:** Supervision, Conceptualization. **Derek Elsworth:** Writing – review & editing, Supervision.

Declaration of competing interest

The authors declare that they have no known competing financial interests or personal relationships that could have appeared to influence the work reported in this paper.

Data availability

Data will be made available on request.

Acknowledgments

This work is supported by the National Natural Science Foundation of China (No. 52225402), the China Postdoctoral Science Foundation (Nos. GZC20231306, 2024 M751714) and the Open Fund of State Key Laboratory of Coal Resources and Safe Mining (No. SKLCRSM20KFA04). These supports are gratefully acknowledged. We thank LetPub (www.letpub.com.cn) for its linguistic assistance during the preparation of this manuscript.

Appendix A. Supplementary data

Supplementary data to this article can be found online at https://doi.org/10.1016/j.fuel.2024.133373.

References

[1] Liu J, Chen Z, Elsworth D, Qu H, Chen D. Interactions of multiple processes during CBM extraction: A critical review. Int J Coal Geol 2011;87(3–4):175–89.
[2] Gao Q, Liu J, Huang Y, Li W, Shi R, Leong Y-K, et al. A critical review of coal permeability models. Fuel 2022;326:125124.
[3] Liu S, Harpalani S. Compressibility of sorptive porous media: Part 1. Background and theory. AAPG Bull 2014;98(9):1761–72.
[4] Karacan CÖ. Swelling-induced volumetric strains internal to a stressed coal associated with CO_2 sorption. Int J Coal Geol 2007;72:209–20.
[5] Jia Q, Liu D, Cai Y, Yao Y, Lu Y, Zhou Y. Variation of adsorption effects in coals with different particle sizes induced by differences in microscopic adhesion. Chem Eng J 2023;452:139511.
[6] Krevor S, de Coninck H, Gasda SE, Ghaleigh NS, de Gooyert V, Hajibeygi H, et al. Subsurface carbon dioxide and hydrogen storage for a sustainable energy future. Nat Rev Earth Environ 2023;4:102–18.
[7] Moore TA. Coalbed methane: A review. Int J Coal Geol 2012;101:36–81.
[8] Zhang H, Liu J, Elsworth D. How sorption-induced matrix deformation affects gas flow in coal seams: A new FE model. Int J Rock Mech Min Sci 2008;45:1226–36.
[9] Liu S, Harpalani S. Permeability prediction of coalbed methane reservoirs during primary depletion. Int J Coal Geol 2013;113:1–10.
[10] Xue Y, Ranjith PG, Dang F, Liu J, Wang S, Xia T, et al. Analysis of deformation, permeability and energy evolution characteristics of coal mass around borehole after excavation. Nat Resour Res 2020;29:3159–77.
[11] Fan C, Elsworth D, Li S, Zhou L, Yang Z, Song Y. Thermo-hydro-mechanical-chemical couplings controlling CH4 production and CO_2 sequestration in enhanced coalbed methane recovery. Energy 2019;173:1054–77.
[12] Biot MA. General theory of three-dimensional consolidation. J Appl Phys 1941;12:155–64.
[13] Zhao Z, Chen S, Chen Y, Yang Q. On the effective stress coefficient of single rough rock fractures. Int J Rock Mech Min Sci 2021;137:104556.
[14] Terzaghi K. Theoretical soil mechanics[M]. INC; 1943.
[15] Saurabh S, Harpalani S. The effective stress law for stress-sensitive transversely isotropic rocks. Int J Rock Mech Min Sci 2018;101:69–77.
[16] Laubach SE, Marrett RA, Olson JE, Scott AR. Characteristics and origins of coal cleat A review. Int J Coal Geol 1998;35:175–207.
[17] Warplnskl NR, Teufel LW. Determination of the effective-stress law for permeability and deformation in low-permeability rocks. SPE Form Eval 1992;7:123–31.
[18] Zhao Y, Zhao Y, Liu J, Wei M, Huang Y, Jiang C. Coal permeability behaviors and non-uniform deformations under various boundary conditions: Part 2 – modelling study. Fuel 2023;343:127914.
[19] Shi R, Liu J, Wei M, Elsworth D, Wang X. Mechanistic analysis of coal permeability evolution data under stress-controlled conditions. Int J Rock Mech Min Sci 2018;110:36–47.
[20] Shi R, Liu J, Wang X, Wei M, Elsworth D. A critical analysis of shale laboratory permeability evolution data. Energy 2021;236:121405.
[21] Zhao Y, Cui D, Liu J, Wei M, Liu Y. Evolution of coal permeability under constant effective stresses: Direct measurements and numerical modeling. Energy Fuel 2021;35:15489–501.
[22] Pan Z, Connell LD. A theoretical model for gas adsorption-induced coal swelling. Int J Coal Geol 2007;69:243–52.
[23] Palmer I. Permeability changes in coal: Analytical modeling. Int J Coal Geol 2009;77:119–26.
[24] Zhu WC, Wei CH, Liu J, Qu HY, Elsworth D. A model of coal–gas interaction under variable temperatures. Int J Coal Geol 2011;86:213–21.
[25] Harpalani S, Chen G. Influence of gas production induced volumetric strain on permeability of coal. Geotech Geol Eng 1997;15:303–25.
[26] Zhao Y, Zhao Y, Liu J, Wei M, Cui D, Gao S. Coal permeability behaviors and non-uniform deformations under various boundary conditions: Part 1 – Experimental observations. Fuel 2023;341:127649.
[27] Kumar H, Elsworth D, Liu J, Pone D, Mathews JP. Optimizing enhanced coalbed methane recovery for unhindered production and CO_2 injectivity. Int J Greenhouse Gas Control 2012;11:86–97.
[28] Harpalani S, Schraufnagel RA. Shrinkage of coal matrix with release of gas and its impact on permeability of coal. Fuel 1990;69:551–6.
[29] Harpalani S, Schraufnagel RA. Measurement of parameters impacting methane recovery from coal seam. Int J Min Geol Eng 1990;8:369–84.
[30] Jessen K, Tang G-Q, Kovscek AR. Laboratory and simulation investigation of enhanced coalbed methane recovery by gas injection. Transp Porous Media 2007;73:141–59.
[31] Siriwardane H, Haljasmaa I, McLendon R, Irdi G, Soong Y, Bromhal G. Influence of carbon dioxide on coal permeability determined by pressure transient methods. Int J Coal Geol 2009;77:109–18.
[32] Pini R, Ottiger S, Burlini L, Storti G, Mazzotti M. CO_2 storage through ECBM recovery: An experimental and modeling study. Energy Procedia 2009;1:1711–7.
[33] Meng Z, Li G. Experimental research on the permeability of high-rank coal under a varying stress and its influencing factors. Eng Geol 2013;162:108–17.
[34] Mitra A, Harpalani S, Liu S. Laboratory measurement and modeling of coal permeability with continued methane production: Part 1 – Laboratory results. Fuel 2012;94:110–6.
[35] Feng R, Harpalani S, Pandey R. Laboratory measurement of stress-dependent coal permeability using pulse-decay technique and flow modeling with gas depletion. Fuel 2016;177:76–86.
[36] Liu S, Harpalani S. Evaluation of in situ stress changes with gas depletion of coalbed methane reservoirs. J Geophys Res Solid Earth 2014;119:6263–76.
[37] Ding Z, Jia J, Feng R. Effect of the vertical stress on CO_2 flow behavior and permeability variation in coalbed methane reservoirs. Energy Sci Eng 2019;7:1937–47.
[38] Li Y, Tang D, Xu H, Meng Y, Li J. Experimental research on coal permeability: The roles of effective stress and gas slippage. J Nat Gas Sci Eng 2014;21:481–8.
[39] Pan Z, Connell LD, Camilleri M. Laboratory characterisation of coal reservoir permeability for primary and enhanced coalbed methane recovery. Int J Coal Geol 2010;82(3–4):252–61.
[40] Harpalani S, Chen G. Influence of gas production induced volumetric strain on permeability of coal. Geotech Geol Eng 1997;15(4):303–25.
[41] Chen Z, Pan Z, Liu J, Connell LD, Elsworth D. Effect of the effective stress coefficient and sorption-induced strain on the evolution of coal permeability: Experimental observations. Int J Greenhouse Gas Control 2011;5(5):1284–93.
[42] Anggara F, Sasaki K, Sugai Y. The correlation between coal swelling and permeability during CO_2 sequestration: A case study using Kushiro low rank coals. Int J Coal Geol 2016;166:62–70.

[43] Arnold JG, Allen PM, Bernhardt G. A comprehensive surface-groundwater flow model. J Hydrol 1993;142(1–4):47–69.
[44] Levine JR. Model study of the influence of matrix shrinkage on absolute permeability of coal bed reservoirs. Geol Soc Lond Spec Publ 1996;109(1):197–212.
[45] Connell LD, Lu M, Pan Z. An analytical coal permeability model for triaxial strain and stress conditions. Int J Coal Geol 2010;84(2):103–14.
[46] Wu Y, Liu J, Elsworth D, Chen Z, Connell L, Pan Z. Dual poroelastic response of a coal seam to CO_2 injection. Int J Greenhouse Gas Control 2010;4(4):668–78.
[47] Wang K, Zang J, Wang G, Zhou A. Anisotropic permeability evolution of coal with effective stress variation and gas sorption: Model development and analysis. Int J Coal Geol 2014;130:53–65.
[48] Liu H, Rutqvist J. A new coal-permeability model: Internal swelling stress and fracture–matrix interaction. Transp Porous Media 2009;82:157–71.
[49] Fathi E, Akkutlu IY. Matrix heterogeneity effects on gas transport and adsorption in coalbed and shale gas reservoirs. Transp Porous Media 2009;80:281–304.
[50] Gross L, Shaw S. Numerical investigations on mapping permeability heterogeneity in coal seam gas reservoirs using seismo-electric methods. J Geophys Eng 2016;13:S50–8.
[51] Liu M, Shabaninejad M, Mostaghimi P. Impact of mineralogical heterogeneity on reactive transport modelling. Comput Geosci 2017;104:12–9.
[52] Mikelić A, Wheeler MF. Theory of the dynamic Biot-Allard equations and their link to the quasi-static Biot system. J Math Phys 2012;53:203–22.
[53] Selvadurai APS. The Biot coefficient for a low permeability heterogeneous limestone. Contin Mech Thermodyn 2018;31:939–53.
[54] Liu J, Chen Z, Elsworth D, Miao X, Mao X. Linking gas-sorption induced changes in coal permeability to directional strains through a modulus reduction ratio. Int J Coal Geol 2010;83(1):21–30.
[55] Hol S, Gensterblum Y, Massarotto P. Sorption and changes in bulk modulus of coal — experimental evidence and governing mechanisms for CBM and ECBM applications. Int J Coal Geol 2014;128–129:119–33.
[56] Sang G, Elsworth D, Liu S, Harpalani S. Characterization of swelling modulus and effective stress coefficient accommodating sorption-induced swelling in coal. Energy Fuel 2017;31:8843–51.
[57] Cui X, Bustin RM. Volumetric strain associated with methane desorption and its impact on coalbed gas production from deep coal seams. AAPG Bull 2005;89:1181–202.
[58] Zhu WC, Wei CH, Liu J, Xu T, Elsworth D. Impact of gas adsorption induced coal matrix damage on the evolution of coal permeability. Rock Mech Rock Eng 2013;46:1353–66.
[59] Li C, Dong L, Xu X, Hu P, Tian J, Zhang Y, et al. Theoretical and experimental evaluation of effective stress-induced sorption capacity change and its influence on coal permeability. J Geophys Eng 2017;14:654–65.
[60] Wei M, Liu J, Elsworth D, Li S, Zhou F. Influence of gas adsorption induced non-uniform deformation on the evolution of coal permeability. Int J Rock Mech Min Sci 2019;114:71–8.
[61] Yang X, Zhang H, Wu W, Gong Z, Yuan W, Feng X, et al. Gas migration in the reservoirs of ultra-low porosity and permeability based on an improved apparent permeability model. J Pet Sci Eng 2020;185:106614.
[62] Wang X, Zhou H, Zhang L, Preusse A, Xie S, Hou W. Research on damage-based coal permeability evolution for the whole stress–strain process considering temperature and pore pressure. Geomech Geophys Geo-Energy Geo-Resour 2022;8(5):1–14.
[63] Liu T, Lin B, Yang W. Impact of matrix–fracture interactions on coal permeability: Model development and analysis. Fuel 2017;207:522–32.
[64] Peng Y, Liu J, Wei M, Pan Z, Connell LD. Why coal permeability changes under free swellings: New insights. Int J Coal Geol 2014;133:35–46.
[65] Liu Z, Liu J, Pan P, Elsworth D, Wei M, Shi R. Evolution and analysis of gas sorption-induced coal fracture strain data. Pet Sci 2020;17(2):376–92.
[66] Wei X, Wang G, Massarotto P, Golding SD, Rudolph V. A review on recent advances in the numericalsimulation for coalbed-methane-recovery process. SPE Reserv Eval Eng 2007;10:657–66.
[67] Tan Y, Pan Z, Liu J, Zhou F, Connell LD, Sun W, et al. Experimental study of impact of anisotropy and heterogeneity on gas flow in coal. Part II: Permeability. Fuel 2018;230:397–409.
[68] Wollenweber J, Alles S, Busch A, Krooss BM, Stanjek H, Littke R. Experimental investigation of the CO_2 sealing efficiency of caprocks. Int J Greenhouse Gas Control 2010;4:231–41.
[69] Wang L, Chen Z, Wang C, Elsworth D, Liu W. Reassessment of coal permeability evolution using steady-state flow methods: The role of flow regime transition. Int J Coal Geol 2019;211:103210.
[70] Fischer GJ. The Determination of permeability and storage capacity: pore pressure oscillation.ethod. Int Geophys 1992:187–211.
[71] Heller K, Bruining H, Smeulders D. Permeability obtained from pressure oscillation experiments. Part I, one phase flow 2002;47:201–7.
[72] Wei M, Liu J, Shi R, Elsworth D, Liu Z. Long-term evolution of coal permeability under effective stresses gap between matrix and fracture during CO_2 injection. Transp Porous Media 2019;130:969–83.
[73] Zhao Y, Zhao Y, Wei M, Liu J, Cui D. A new experimental system and method for periodically measuring permeability and strains of coal. Gas Sci Eng 2023;110:204909.
[74] Pan Z, Connell LD. Modelling permeability for coal reservoirs: A review of analytical models and testing data. Int J Coal Geol 2012;92:1–44.
[75] Shi R, Liu J, Wang X, Elsworth D, Liu Z, Wei M, et al. Experimental observations of heterogeneous strains inside a dual porosity sample under the influence of gas-sorption: A case study of fractured coal. Int J Coal Geol 2020;223:103450.
[76] Danesh N, Chen Z, Connell LD, Kizil MS, Pan Z, Aminossadati SM. Characterisation of creep in coal and its impact on permeability: An experimental study. Int J Coal Geol 2017;173:200–11.
[77] Liu S, Harpalani S. Compressibility of sorptive porous media: Part 2. Exper study coal. AAPG Bull 2014;98(9):1773–88.
[78] Lv Z, Liu P, Zhao Y. Experimental study on the effect of gas adsorption on the effective stress of coal under triaxial stress. Transp Porous Media 2021;137(2):365–79.
[79] Li B, Yang K, Ren C, Li J, Xu J. An adsorption-permeability model of coal with slippage effect under stress and temperature coupling condition. J Nat Gas Sci Eng 2019;71:102983.
[80] Shen S, Li X, Fang Z, Shen N, Perera MSA. Effect of gas adsorption on the application of the pulse-decay technique. Geofluids 2020;2020:1–11.
[81] Liu J, Chen Z, Elsworth D, Miao X, Mao X. Evolution of coal permeability from stress-controlled to displacement-controlled swelling conditions. Fuel 2011;90(10):2987–97.